Macromolecules

ARTICLE

pubs.acs.org/Macromolecules

Solid-State Structure and Crystallization in Double-Crystalline Diblock Copolymers of Linear Polyethylene and Hydrogenated Polynorbornene

Sheng Li, Sasha B. Myers,† and Richard A. Register*

Department of Chemical and Biological Engineering, Princeton University, Princeton, New Jersey 08544, United States

Supporting Information

ABSTRACT: Double-crystalline diblock copolymers of linear polyethylene (LPE) and hydrogenated polynorbornene (hPN) are synthesized, and their crystallization behavior and morphology are examined using small-angle (SAXS) and wide-angle X-ray scattering (WAXS). In symmetric hPN/LPE diblocks with molecular weights above 50 kg/mol, the hPN block has previously been shown to crystallize first and set the solid-state microstructure. Two-dimensional WAXS on hand-drawn fiber specimens reveals that the LPE crystals formed in confinement stack orthogonally to the hPN crystals. By adjusting total molecular weight, the order of block crystallization may be reversed, even while holding the block length ratio fixed. At a diblock molecular weight of 20 kg/mol, simultaneous time-resolved SAXS/WAXS reveals that the LPE block crystallizes first, even when LPE is the minority component, and restricts hPN to crystallize between the LPE lamellae. The relative orientation of the LPE and hPN crystals in the lower molecular weight diblocks is examined by modeling changes in the SAXS primary peak intensity on cooling two diblocks through the hPN crystal−crystal transition, where hPN densifies as it adopts a rotationally ordered crystal structure. Only a perpendicular stacking of hPN and LPE crystals consistently yields the large reduction in primary SAXS peak intensity observed for both diblocks. Thus, even though the templating block switches from hPN to LPE as the diblock molecular weight is reduced, the orthogonal stacking motif is retained for both high- and low-molecular-weight copolymers.

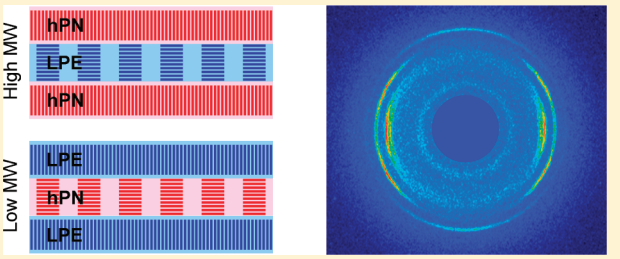

INTRODUCTION

One of the most interesting aspects of block copolymers is that they can self-assemble into different microstructures depending on block length ratio and segregation strength.[1] When the block copolymer contains segments that are crystallizable, microphase separation may also be driven by block crystallization, resulting in an even richer array of solid-state morphologies.[2−4] Crystallization in diblock copolymers containing one crystallizable and one amorphous block has been studied extensively. When crystallization takes place from a disordered[5,6] or weakly segregated melt,[7,8] the resulting solid-state morphology is typically alternating crystalline/amorphous lamellae, regardless of the copolymer composition. In this case, microphase separation in the solid state is driven by crystallites' tendency to organize themselves in lamellae; therefore, the crystals lie parallel to the lamellar microdomains which they form.[5,9,10] When the melt is strongly segregated,[11,12] or when one block vitrifies prior to crystallization of the other,[13,14] crystallization may be confined within the existing microdomains, such that the melt morphology is preserved in the solid state. This type of confined crystallization also affects crystal orientation—most commonly, the fast growth direction of the crystals preferentially aligns with the long axis of the microdomain.[15−17] The orientation of crystals formed in a confined environment can also be manipulated through the crystallization temperature. In studies of the crystallization of poly(ethylene oxide) within lamella-forming poly(ethylene oxide-*b*-styrene) diblock copolymers, as the crystallization temperature is increased, the resulting crystal orientation is found to tilt from the lamellar surface, leading to a stem orientation that is parallel, then inclined, and then perpendicular with respect to the lamellar microdomains.[18−20]

As the number of different crystallizable units in a block copolymer increases, its crystalline morphology becomes even more complex. The subject of crystallization in block copolymers containing two chemically distinct crystallizable blocks has attracted much interest in recent years.[21] In general, two types of crystallization may be expected in double-crystalline diblock copolymers. In the first type, the melting temperatures of the two blocks are far apart, as are their freezing temperatures, so that the component with the higher melting/freezing temperature is always the first to crystallize,[22−26] thereby setting up a structural template within which the lower-melting-temperature component subsequently crystallizes. An example of such a double-crystalline diblock copolymer system is poly(ε-caprolactone-*b*-ethylene), PCL/PE. The melting temperature of the PCL block is about 60 °C, while that of the PE block is about 100 °C; the PE block is always the first to crystallize, yielding a crystalline/amorphous lamellar microstructure.[24] The PCL block subsequently

Received: August 25, 2011
Revised: October 1, 2011
Published: October 17, 2011

also crystallizes, and depending on the crystallization temperature employed, PCL crystallization may either be confined between, or break out from, the PE crystalline lamellae.[24,25] When crystallization of the PCL block is confined, the orientation of the resulting crystals is strongly influenced by both crystallization temperature and PCL domain thickness,[26] similar to crystallization under glassy confinement in crystalline/glassy diblock copolymers.

In the second type of double-crystalline diblock, the melting temperatures of the two blocks are close to each other, such that upon cooling the two blocks engage in competitive crystallization.[27−32] In such a diblock copolymer, it is not obvious which component will crystallize first, and there exists the opportunity to tune the sequence of crystallization and the resulting crystalline morphology by adjustment of macromolecular architecture and/or processing conditions. One diblock copolymer system where the two blocks share comparable melting temperatures is poly(ε-caprolactone-*b*-ethylene oxide), PCL/PEO,[29] in which the crystallization sequence may be tuned by changing crystallization temperature[30] or block length ratio.[31,32]

We have recently investigated double-crystalline diblock copolymers composed of linear polyethylene (LPE), also known as high-density polyethylene, and hydrogenated polynorbornene (hPN).[33] Homopolymers of LPE and hPN both exhibit high degrees of crystallinity and similar melting temperatures: $T^0_{m,LPE}$[34,35] = 141−142 °C, $w_{c,LPE}$[36] ≈ 75%; $T^0_{m,hPN}$[37] = 156 °C, $w_{c,hPN}$[37] ≈ 80%. Our previous study examined the crystallization sequence and solid-state morphologies in hPN/LPE diblocks of relatively high molecular weight (M_n > 50 kg/mol).[33] In diblocks of symmetric composition, the hPN block crystallized first to set up the overall solid-state microstructure; LPE subsequently crystallized between the hPN lamellae. The crystallization behavior was also tunable via the block length ratio: in hPN-rich diblocks, hPN crystallized first, while in LPE-rich diblocks, LPE crystallized first, which then "triggered" the crystallization of hPN. In the present study, we provide direct evidence regarding the crystal orientation in such higher molecular weight hPN/LPE diblocks; furthermore, we synthesize hPN/LPE diblocks of lower molecular weight and demonstrate the possibility of tuning crystallization sequence by adjusting total molecular weight, in addition to block length ratio. The solid-state microstructure and crystal orientation in these lower molecular weight hPN/LPE diblocks are also investigated and found to resemble those in their higher molecular weight counterparts, though the identities of the templating and confined blocks (hPN vs LPE) are interchanged.

EXPERIMENTAL SECTION

Materials. The hPN/LPE diblocks were synthesized by sequential living ring-opening metathesis polymerization (ROMP) of norbornene and cyclopentene, followed by hydrogenation over palladium supported on calcium carbonate ($Pd^0/CaCO_3$, 5 wt % Pd^0, Alfa Aesar). The ROMP reactions were initiated with the Schrock-type catalyst 2,6-diisopropylphenylimidoneophylidenemolybdenum(VI) bis(*tert*-butoxide). The norbornene block was synthesized first, followed by the addition of trimethylphosphine (PMe_3) and polymerization of the cyclopentene block. The details of diblock copolymer synthesis have been described previously.[33]

It is important to note that when ROMP is initiated by the Schrock-type Mo catalyst, narrow-distribution polynorbornene (PN) can be produced either with or without PMe_3, which moderates the propagation rate. However, PMe_3 also alters the tacticity of the PN, leading to significant differences in the thermal properties of the hydrogenated derivative (hPN).[38] The PN block in the current study was synthesized in the absence of PMe_3, thus imparting to the hPN a crystal−crystal transition temperature (T_{cc}) that is easily separable from its melting temperature (T_m) as well as a relatively small hysteresis in T_{cc} upon heating and cooling. Notable changes occur in the X-ray scattering profile at T_{cc}; as elaborated below, these changes greatly aid in determining the relative crystal orientation in these double-crystalline diblock copolymers.

Table 1. Molecular Characteristics of Block Copolymers and Homopolymers

sample code (hPN/LPE)	hPN block M_n (g/mol)	hPN block M_w/M_n	LPE block M_n (g/mol)	diblock M_w/M_n	volume fraction hPN at 160 °C (f_{hPN})
9/9	9 300	1.13	8 600	1.09	0.49
6/12	6 000	1.16	11 600	1.11	0.31
11/6	10 900	1.10	6 300	1.11	0.60
26/26	26 300	1.07	25 800	1.11	0.47
hPN	61 000	1.11			1
LPE			20 000	1.07	0

The molecular characteristics of the diblock copolymers examined are listed in Table 1. Characterization was conducted on the soluble, unsaturated poly(norbornene-*b*-cyclopentene) (PN/PCP) diblocks, following the same protocols used previously to characterize the higher molecular weight diblocks.[33] Polymer molecular weights and polydispersities were determined by gel permeation chromatography (GPC) in tetrahydrofuran (THF). Diblock composition was measured by ^{1}H NMR, using the olefinic protons from both repeat units and the methine protons from the PN block. Volume fractions of hPN in the melt at 160 °C, f_{hPN}, were calculated with known mass densities of hPN (0.879 g/cm^3, see also Supporting Information)[39] and LPE (0.774 g/cm^3).[40] The diblocks are referred to by their hPN/LPE block molecular weights in kg/mol. The lower molecular weight hPN/LPE diblocks, which are the focus of the present work, are complemented by previously studied hPN[37] and LPE[36] homopolymers as well as a higher molecular weight diblock, hPN/LPE 26/26,[33] whose characterization data are also included in Table 1.

Measurements. Differential scanning calorimetry (DSC) measurements employed a Perkin-Elmer DSC 7 equipped with an intracooler and calibrated with indium and tin. For each polymer, a ca. 10 mg specimen was prepared, and the heating and cooling scans were acquired at 10 °C/min. For fiber X-ray diffraction, fibers of the diblock copolymer were drawn manually by heating a small quantity of the material on a hot plate above its melting point, grabbing the molten polymer with tweezers, and then pulling away at a steady speed. Fibers were arranged into a bundle sufficiently large to cover the X-ray beam, secured between two pieces of polyimide tape. Fiber diffraction measurements employed a Statton pinhole camera system previously described,[41] equipped with hot stage, using Cu Kα radiation (λ = 0.1542 nm). Diffraction patterns were recorded on Kodak image plates read by a GE Biosciences Storm 820 scanner. The positions of the reflections in the diffraction patterns were calibrated with high-density polyethylene.

Time- and temperature-resolved simultaneous small-angle (SAXS) and wide-angle X-ray scattering (WAXS) data were collected on isotropic specimens at the DuPont−Northwestern−Dow Collaborative Access Team (DND-CAT) beamline (5ID-D) at the Advanced Photon Source, Argonne National Laboratory. The X-ray energy was set at 17 keV (λ = 0.0729 nm). SAXS data were collected on a MAR USA CCD camera at a sample-to-detector distance of 8 m, while a quadrant of

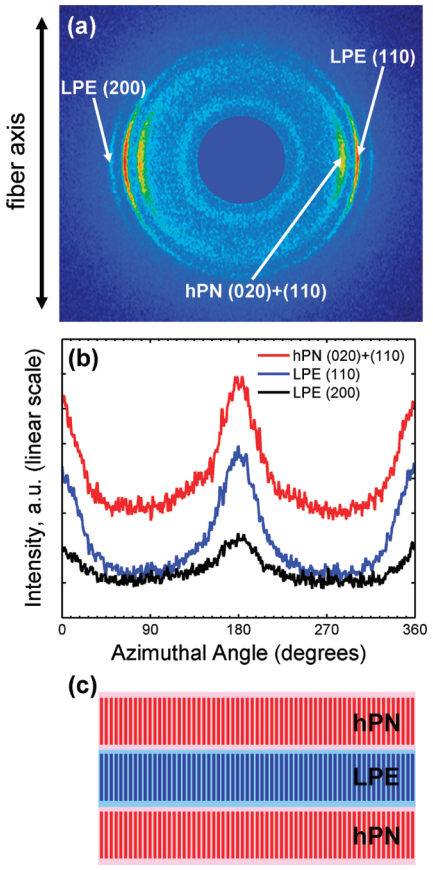

Figure 1. (a) Room-temperature X-ray diffraction pattern for hPN/LPE 26/26 fiber specimen, previously annealed below T_m of both the hPN and LPE blocks. (b) Azimuthal intensity profiles integrated over the angular range corresponding to the overlapping (020) and (110) peaks of monoclinic hPN (red) or (110) (blue) or (200) (black) peaks of orthorhombic LPE. (c) Schematic of the orientation of the hPN and LPE crystals within the lamellar microdomains, with crystal stems indicated by line segments.

WAXS data was simultaneously collected on a Roper Scientific CCD camera at a sample-to-detector distance of 14 cm. All X-ray scattering data were corrected for incident beam intensity, transmittance, and specimen thickness; the isotropic two-dimensional scattering patterns were then converted to one-dimensional intensity traces. The polymer samples were enclosed inside standard aluminum DSC pans (TA Instruments), held in a Linkam DSC 600 hot stage. The temperature profile employed was heating from 20 to 160 °C at 20 °C/min; 1 min hold at 160 °C; quenching at 40 °C/min to an isothermal crystallization temperature, T_c; 10 min hold at T_c; cooling to 20 °C at 20 °C/min.

RESULTS AND DISCUSSION

Higher Molecular Weight Diblocks. In a previous publication,[33] we reported that in symmetric diblock copolymers of hPN and LPE with molecular weights above 50 kg/mol, hPN is the first block to crystallize; hPN crystallization thus sets up the primary lamellar structure, and the LPE block subsequently crystallizes between hPN lamellae. In that case, isotropic specimens were employed; we inferred that the LPE crystals stack orthogonally to the hPN crystals from changes in the SAXS primary peak intensity. Here we directly investigate the crystalline morphology in one of these higher molecular weight diblocks after orienting the crystals via fiber drawing. The room-temperature fiber X-ray diffraction pattern for hPN/LPE 26/26 is shown in Figure 1. Prior to collecting the data in Figure 1, the drawn fiber specimen was annealed at $T = 132$ °C, just below the melting points of both hPN and LPE blocks, for 20 min to improve its degree of crystallinity. The 2D scattering pattern and the azimuthal intensity plot indicate that both the overlapping (020) and (110) reflections associated with monoclinic hPN and the (110) and (200) reflections associated with orthorhombic LPE are concentrated along the equator. This indicates that the crystals are oriented as schematized in Figure 1c, where both the hPN and LPE crystal stems are aligned in the direction of the fiber axis, parallel to the lamellar microdomain normal.

In creating the fiber specimen for which data are shown in Figure 1, both the hPN and LPE blocks were crystallized under tension, which might be expected to heavily influence the crystal orientation, even for the block which is second to crystallize (LPE). To recreate the LPE crystal orientation that would be observed in quiescent crystallization, while still preserving the fiber orientation of the structure-templating hPN block, the LPE crystals were melted and recrystallized. Specifically, the as-drawn and annealed hPN/LPE block copolymer fiber for which data are shown in Figure 1 was first heated to 138 °C, where LPE is molten (see Supporting Information), while hPN remains largely crystalline. The partially melted fiber was then cooled to recrystallize the LPE block in the presence of the templating hPN crystal framework, but in the absence of any stress. The diffraction pattern for the recrystallized fiber specimen, shown in Figure 2, is qualitatively different from that of the as-drawn and annealed fiber. As shown in Figure 2a,b, after partial melting and recrystallization, the LPE (110) reflection now splits across the equator, with an azimuthal split angle $\tau \cong 60°$, while the LPE (200) reflections concentrate on the meridian, with $\tau = 180°$. This new fiber pattern is consistent with the LPE crystals stacking orthogonally to the hPN crystalline lamellae, as illustrated in Figure 2c. Note that if the *c*-axis of the LPE orthorhombic unit cell were perfectly perpendicular to the fiber axis (thus perpendicular to the hPN *c*-axis), the LPE (200) reflection would not appear, and the LPE (110) reflection should show $\tau = 68.8°$; the difference seen in the measured value of $\tau \cong 60°$ for the LPE (110) reflection, and the presence of a visible LPE (200) reflection, indicates some tilt of the *c*-axis away from the lamellar interface.

Comparing the X-ray diffraction patterns shown in Figures 1 and 2, we find that when the double-crystalline diblock crystallizes under tension, the resulting crystalline morphology mainly reflects the processing conditions, and the crystal stems align in the direction of the applied external force (i.e., the fiber axis). When the second-to-crystallize LPE block was allowed to recrystallize quiescently, its stem orientation is mainly influenced by the presence of the confining structure created by the existing hPN crystalline lamellae. Similar to the case where the crystallizing block is confined between glassy lamellae,[17,42] the crystals orient their stems perpendicular to the lamellar normal to alleviate the incommensurability between the preferred crystal/amorphous repeat distance of LPE and the LPE layer thickness set by crystallization of the hPN block.

Lower Molecular Weight Diblocks. Having established the crystallization behavior and morphology of hPN/LPE diblock copolymers of relatively high molecular weights, we then moved to examine the possibility of tuning the sequence of crystallization in these materials by adjusting molecular weight. Previous studies

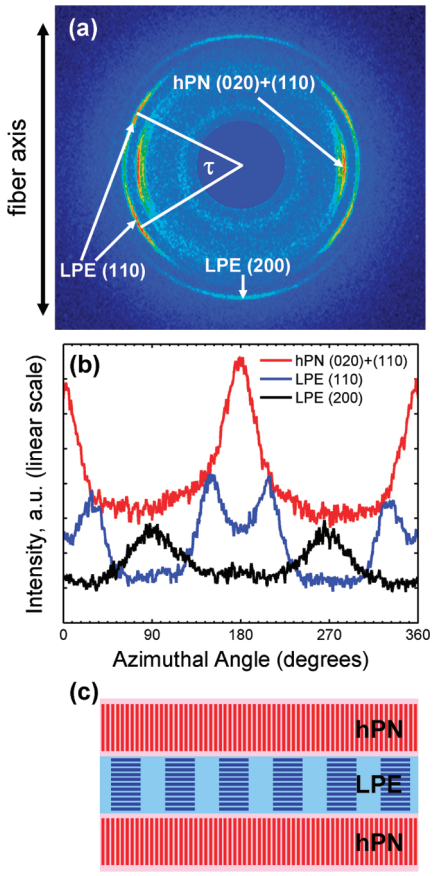

Figure 2. (a) Room-temperature X-ray diffraction pattern for partially melted (at 138 °C) and then recrystallized hPN/LPE 26/26 fiber specimen. (b) Azimuthal intensity profiles integrated over the angular range corresponding to the overlapping (020) and (110) peaks of monoclinic hPN (red) or (110) (blue) or (200) (black) peaks of orthorhombic LPE. (c) Schematic of the orientation of the hPN and LPE crystals within the lamellar microdomains, with crystal stems indicated by line segments.

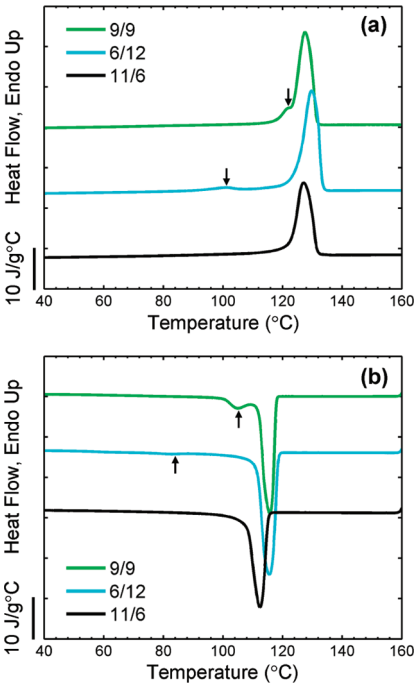

Figure 3. DSC heating (a) and cooling (b) thermograms for lower molecular weight hPN/LPE diblock copolymers, acquired at 10 °C/min.

have shown that hPN homopolymer exhibits an equilibrium melting temperature of 156 °C,[37] while a 4 kg/mol hPN, which forms extended-chain crystals, has a melting temperature of 128 °C.[6] LPE has an equilibrium melting temperature of 141−142 °C,[34,35] while the melting temperature drops only modestly, to 128 °C, for extended-chain crystals of 3 kg/mol LPE.[43] These figures indicate that the melting temperature of hPN exhibits a steeper dependence on molecular weight than does the melting temperature of LPE, at least for extended-chain crystals. If this trend also holds for crystallization (freezing) temperature, and for folded-chain as well as extended-chain crystals, then at sufficiently low diblock molecular weight the crystallization temperature of LPE should exceed the crystallization temperature of hPN; in this scenario, LPE would be the structure-templating block, thus reversing the order of crystallization relative to that in higher molecular weight diblocks such as hPN/LPE 26/26.

To test this premise, three hPN/LPE diblock copolymers with total molecular weights around 20 kg/mol were examined. All three exhibit featureless SAXS patterns (presented subsequently) in the melt at 160 °C, indicating that the melt phases are homogeneous. As the polymer is cooled, both the hPN and LPE blocks crystallize, as demonstrated by WAXS (also presented subsequently). The melting and crystallization of the blocks can be detected via DSC during heating and cooling scans, as illustrated in Figure 3. For hPN/LPE 11/6, only a single peak is evident on either heating or cooling, suggesting that the two blocks' melting and crystallization processes heavily overlap; however, as the hPN block length is reduced (in hPN/LPE 9/9), a low-temperature shoulder emerges, which becomes a resolved peak at even lower temperature as the hPN block length is reduced further (in hPN/LPE 6/12). Note that hPN homopolymer has a heat of fusion some 3-fold smaller than LPE homopolymer.[37] While the origin of these subsidiary peaks/shoulders, indicated with arrows in Figure 3, cannot be determined unambiguously by DSC alone, simultaneous synchrotron WAXS/DSC indicates that these features reflect the melting/crystallization of the hPN block; a direct comparison of the heating thermograms and selected WAXS patterns is given for hPN/LPE 9/9 and 6/12 in the Supporting Information. Consequently, we employed synchrotron-based simultaneous time- and temperature-resolved SAXS and WAXS to reveal the melting and crystallization behavior of these lower molecular weight diblock copolymers.

Symmetric Diblock Copolymer hPN/LPE 9/9. The isothermal crystallization of hPN/LPE 9/9 at 122 °C is examined in Figure 4. The WAXS data, in Figure 4a, show that the (110) and (200) reflections of the usual orthorhombic unit cell of LPE grow in intensity over time, while there is a complete absence of any WAXS reflections associated with hPN crystallization. This clearly indicates that for hPN/LPE 9/9 LPE is the first block to crystallize. Comparing this observation to the crystallization sequence found[33] in hPN/LPE 26/26 confirms that reducing the total molecular weight at fixed composition can indeed lead to a reversal in the block crystallization order in hPN/LPE diblocks.

The simultaneously acquired SAXS data are shown in Figure 4b, where $q = (4\pi/\lambda) \sin \theta$; λ is the radiation wavelength,

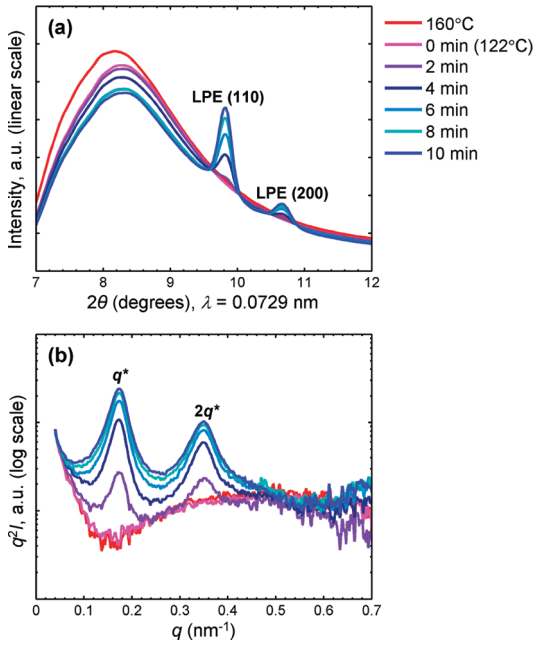

Figure 4. Simultaneously acquired WAXS (a) and SAXS (b) patterns for hPN/LPE 9/9 at T_c = 122 °C after quenching from the melt at 160 °C.

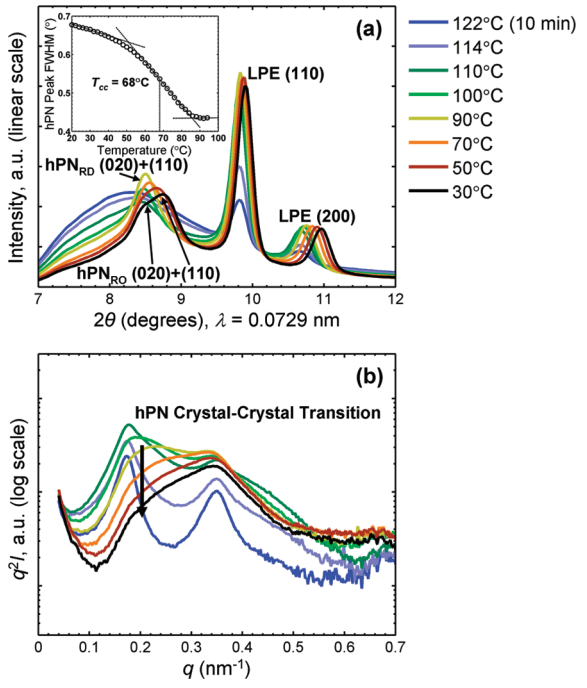

Figure 5. Simultaneously acquired WAXS (a) and SAXS (b) patterns for hPN/LPE 9/9 during further cooling to 30 °C from the isothermal crystallization temperature of 122 °C. The effect that the crystal−crystal transition of the hPN block from a rotationally disordered (RD) to a rotationally ordered (RO) phase has upon the first-order SAXS peak is marked; both phases are monoclinic. The inset in (a) shows the full width at half-maximum (fwhm) of the hPN (020) + (110) reflections as a function of temperature.

and 2θ is the scattering angle. The intensity profiles shown are q^2-corrected to account for the lamellar form factor scattering.[44]

The evolution of the SAXS and WAXS intensity profiles indicates the emergence of a microphase-separated structure from an originally homogeneous melt as the LPE block begins to crystallize. This microphase-separated structure has SAXS reflections appearing at integer q ratios, characteristic of a lamellar microstructure. The interlamellar domain spacing, d, determined from the position of the SAXS primary peak is 36 nm.

The WAXS and SAXS data acquired during further cooling of hPN/LPE 9/9 to room temperature are presented in Figure 5. The WAXS data show that upon cooling the hPN block also crystallizes, as indicated by the emergence of the (020) + (110) reflections of the monoclinic unit cell of hPN. At higher temperature, the hPN (020) + (110) reflections are degenerate, but as the temperature drops further, this single reflection broadens and eventually appears as overlapping but distinct (020) and (110) reflections. This transformation in the WAXS pattern reflects changes in the packing of the hPN crystal unit cell.[37,38] At high temperatures, the hPN stems are rotationally disordered (RD) and exhibit a hexagonal packing transverse to the chain axes.[37] As the temperature is lowered, the hexagonal symmetry is broken as the chains adopt a rotationally ordered (RO) structure, where the stems pack more densely, leading to a contraction in the volume of the unit cell by ∼1%.[37,39] To quantify the temperature where this crystal−crystal transition of the hPN block occurs (T_{cc}), the full width at half-maximum (fwhm) of the combined hPN (020) + (110) WAXS reflections is tracked as a function of temperature, as illustrated in the inset of Figure 5a. As the temperature decreases, a step increase in the peak breadth is observed, as the degenerate (020) and (110) reflections split. T_{cc} is then assigned as the midpoint of the transition; for hPN/LPE 9/9, $T_{cc} \cong 68$ °C on cooling at 20 °C/min.

In addition to the changes observed in the WAXS pattern, this hPN crystal−crystal transition also causes significant changes in the SAXS profiles. As illustrated in Figure 5b, as the temperature drops through T_{cc}, a large reduction in the SAXS primary peak intensity is observed. This change in the SAXS profile is not the result of any lamellar-scale structural change but is due to the ∼1% electron density increase that accompanies the hPN crystal−crystal transition. Our efforts to model the SAXS intensity changes to reveal the hPN crystal orientation in these double-crystalline diblocks are discussed in a subsequent section; first, we present SAXS/WAXS results for the other two diblocks introduced in Table 1.

LPE-Rich Diblock Copolymer hPN/LPE 6/12. This diblock has an overall molecular weight similar to hPN/LPE 9/9 but is rich in LPE. WAXS and SAXS data, acquired during a 10 min hold at 122 °C, are presented in Figures 6a and 6b. The WAXS data show that the peaks associated with LPE crystals grow over time while the hPN block remains amorphous, indicating that LPE is again the first component to crystallize. The SAXS data show that LPE crystallization sets the primary lamellar framework of the system, with a d-spacing of 30 nm. The SAXS profiles obtained during isothermal crystallization at 122 °C all contain a prominent minimum centered near q = 0.53 nm^{-1}. This corresponds to a form factor node from lamellae with a thickness of 12 nm,[44,45] which we consider to be the LPE crystals, separated by amorphous layers of less uniform thickness.

Following further cooling of hPN/LPE 6/12 to room temperature, the WAXS data, shown in Figure 6c, confirm that the hPN block also crystallizes. However, when plotting the breadth of the hPN (020) + (110) reflections as a function of temperature (inset), no step increase is observed, and the breadth remains

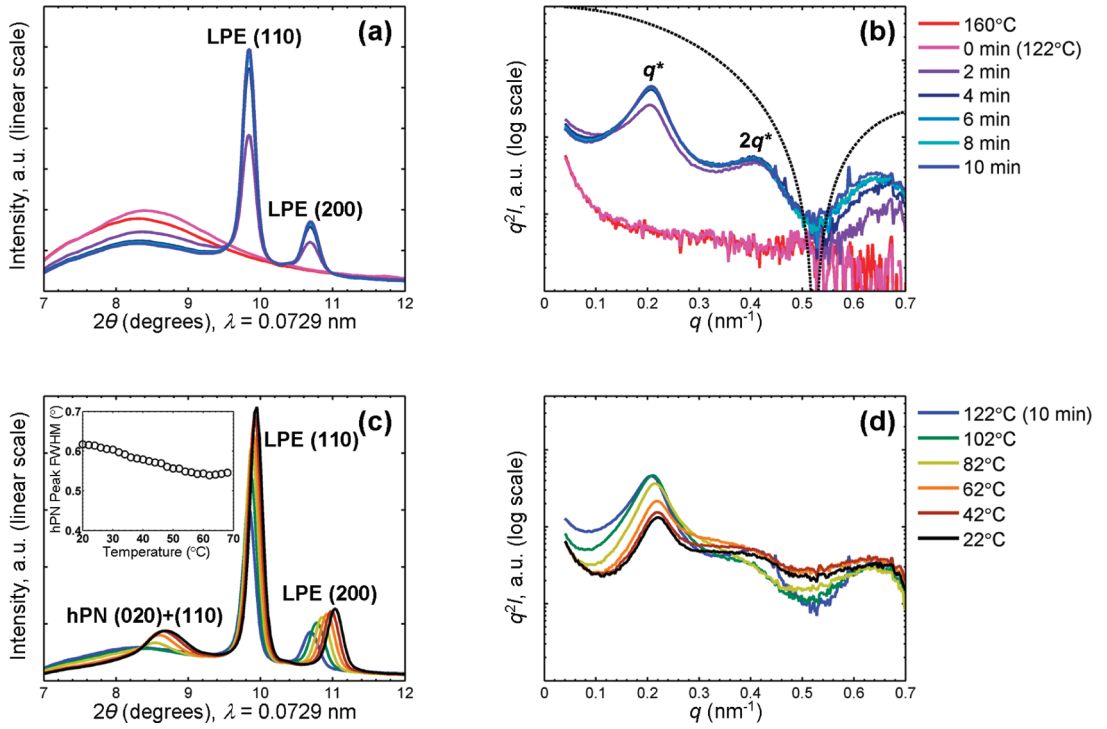

Figure 6. Simultaneously acquired WAXS (a) and SAXS (b) patterns for hPN/LPE 6/12 at T_c = 122 °C after quenching from the melt at 160 °C. The form factor curve for isolated lamellae with a thickness of 12 nm is also shown in (b) as the dotted curve. The WAXS and SAXS patterns acquired during further cooling of the diblock from T_c to 22 °C are shown in (c) and (d), respectively. The inset in (c) shows a plot of the full width at half-maximum (fwhm) of the hPN (020) + (110) reflection as a function of temperature during cooling.

relatively small (<0.62° even at room temperature), suggesting that the hPN crystals remain in the RD phase over the whole temperature range examined. This absence of an hPN crystal−crystal transition is also supported by the SAXS data, which as shown in Figure 6d exhibit a much less dramatic change in the intensity of the primary reflection than in hPN/LPE 9/9, as temperature is lowered. The observed intensity decrease in the SAXS profiles between 82 and 42 °C is consistent with the expected reduction in electron density contrast upon hPN crystallization into the RD phase.

Additionally, since the SAXS profiles acquired during crystallization for hPN/LPE 6/12 are not complicated by an hPN block crystal−crystal transition, the scattering data can be more critically examined to reveal any lamellar-scale rearrangements during crystallization. Figure 6 reveals that as hPN crystallizes, the shape of the profile remains largely unchanged, with merely some additional intensity at q values beyond the primary peak (from the hPN crystals), and a slight shift of the primary peak to higher q as the lamellar spacing contracts (upon both hPN crystallization and cooling). This strongly indicates that the overall lamellar microstructure established by LPE crystallization at 122 °C is preserved through hPN crystallization and that crystallization of the hPN block is confined between the LPE crystalline lamellae.

hPN-Rich Diblock Copolymer hPN/LPE 11/6. In higher molecular weight hPN/LPE diblock copolymers, the identity of the structure-templating block may be changed by large adjustments in the block length ratio,[33] so we also examined an hPN-rich diblock copolymer, hPN/LPE 11/6. The WAXS data for the isothermal crystallization of hPN/LPE 11/6 at 120 °C are presented in Figure 7. At 2 min into the isothermal hold, the first

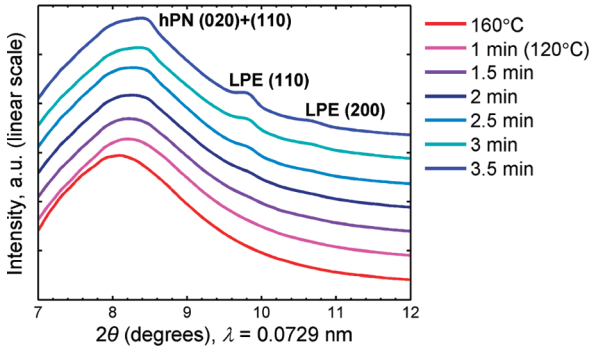

Figure 7. WAXS patterns for hPN/LPE 11/6 acquired at T_c = 120 °C after quenching from the 160 °C melt. WAXS reflections associated with hPN and LPE appear to emerge simultaneously. Successive WAXS patterns are offset vertically for clarity.

sign of block crystallization may be detected; however, the hPN (020) + (110) reflections and the LPE (110) reflection emerge essentially simultaneously. Note that the time resolution of the WAXS frames in Figure 7 is 6 s, far shorter than the time scale of the crystallization process, so the simultaneity of hPN and LPE crystallization is not an artifact of insufficient time resolution.

Consequently, we probed the sequence of crystallization by examining the isothermal crystallization half-time ($t_{1/2}$) as a function of crystallization temperature (T_c), using $t_{1/2}$ values determined by DSC. Shown in Figure 8 are such plots for a number of hPN/LPE diblocks as well as LPE and hPN homopolymers. The isothermal crystallization half-time of LPE homopolymer exhibits a steeper dependence on temperature than does

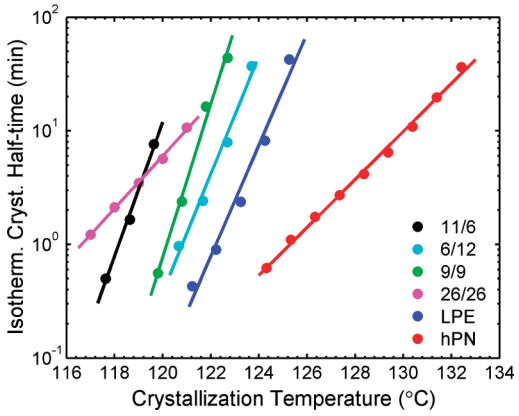

Figure 8. DSC isothermal crystallization half-time as a function of crystallization temperature for the three lower molecular weight hPN/LPE diblocks examined, hPN/LPE 26/26, and the homopolymers of hPN and LPE listed in Table 1. Best-fit lines have the slopes indicated in the text.

hPN homopolymer: a slope of 3.1 $°C^{-1}$ for LPE vs 1.6 $°C^{-1}$ for hPN. Furthermore, this characteristic temperature-dependent crystallization behavior is also observed in diblocks containing both LPE and hPN, where the temperature dependence of the crystallization half-time of a diblock is found to match that of its structure-templating block. hPN/LPE 26/26, which has hPN as its structure-templating block, exhibits a shallow temperature dependence of $t_{1/2}$ (1.7 $°C^{-1}$) similar to hPN homopolymer, while both hPN/LPE 9/9 and 6/12, where the LPE block is templating, have much steeper temperature dependences (4.7 and 3.3 $°C^{-1}$, respectively), similar to LPE homopolymer. The hPN-rich low molecular weight diblock, hPN/LPE 11/6, exhibits a steep temperature dependence (3.9 $°C^{-1}$), similar to that observed in LPE homopolymer and the LPE-templating diblocks hPN/LPE 9/9 and 6/12, thus suggesting that LPE is also the first block to crystallize in hPN/LPE 11/6. This then triggers hPN block crystallization, leading to the near-simultaneous crystallization of the two blocks as observed by WAXS. Related phenomena in double-crystalline diblocks where the crystallization rate of one block is enhanced by prior crystallization of the other block have been reported.[33,46−48] The crystallites generated from the initial crystallization event may serve as nucleation sites for the remaining molten block; moreover, crystallization of the LPE block concentrates the interlamellar "melt" in hPN, effectively increasing its chemical potential and thus driving force to crystallize.

The WAXS and SAXS data collected upon cooling hPN/LPE 11/6 are shown in Figure 9. The diblock was first quenched from the melt to 119 °C, then isothermally crystallized at that temperature for 10 min, and then cooled to room temperature. The WAXS data confirm that both hPN and LPE crystallize upon cooling, and the crystallinities of both blocks are fully developed by the end of the 10 min isothermal hold at 119 °C. Upon further cooling, the hPN block undergoes a clear crystal−crystal transition from the RD to the RO phase. The transition temperature, as illustrated in the inset of Figure 9a, is estimated to occur at 94 °C on cooling at 20 °C/min.

The corresponding SAXS profiles obtained during cooling are shown in Figure 9b. At temperatures above T_{cc}, the SAXS data resemble those for hPN/LPE 6/12, where a microphase-separated lamellar structure with a period d = 37 nm emerges

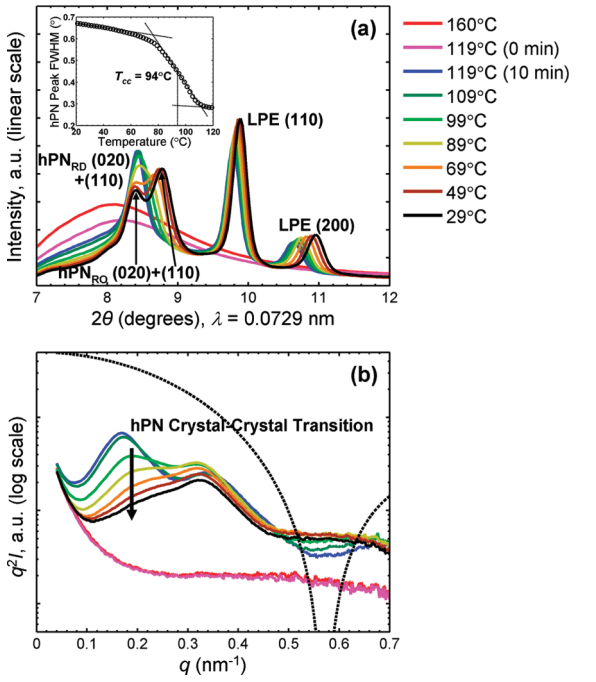

Figure 9. Simultaneously acquired WAXS (a) and SAXS (b) patterns for hPN/LPE 11/6, first quenched from the melt (at 160 °C) to T_c = 119 °C, then isothermally crystallized at T_c for 10 min, and then further cooled to 29 °C. Crystal−crystal transition of the hPN block from the RD phase to the RO phase is marked. The inset in (a) shows the full width at half-maximum (fwhm) of the hPN (020) + (110) reflections as a function of temperature. The form factor curve for isolated lamellae with a thickness of 11 nm is shown in (b) as the dotted curve.

from a homogeneous melt upon LPE crystallization; this lamellar framework is also preserved as hPN crystallinity develops. A minimum in the SAXS profiles is observed near q = 0.58 nm^{-1}, which again corresponds to a form factor node, in this case from lamellae 11 nm thick,[44,45] assigned to the LPE crystals based on the value of d and f_{hPN}. The DSC-determined peak melting temperature (T_m = 127.1 °C from overlapping LPE and hPN endotherms) confirms this assignment as it yields a LPE crystal thickness of 11.5 nm via the Gibbs−Thomson equation.[35,49] The presence of a form factor minimum in the 119 °C (10 min) SAXS pattern for hPN/LPE 11/6 further supports the conclusion that LPE is the first block to crystallize, as hPN/LPE 9/9 and 6/12 also show a similar form factor minimum corresponding to the templating LPE crystals. In homopolymers, the crystals generally have a narrower thickness distribution than the amorphous interlayers separating them,[50] and for our block copolymers we also see that, during isothermal crystallization, the first-to-crystallize block (LPE here) forms crystals with a relatively narrow thickness distribution compared with the initially amorphous interlayers (hPN here). Crystallization of the hPN block in hPN/LPE 11/6, though it follows nearly simultaneously upon LPE crystallization, cannot restructure the lamellar framework established by LPE crystallization. Subsequently, as the material is further cooled through T_{cc} (94 °C), a dramatic reduction in the SAXS primary peak intensity is observed due to the electron density change at the hPN crystal−crystal transition, as in the symmetric diblock hPN/LPE 9/9.

Crystal Orientation in Lower Molecular Weight Diblocks. As shown above, in all three lower molecular weight hPN/LPE

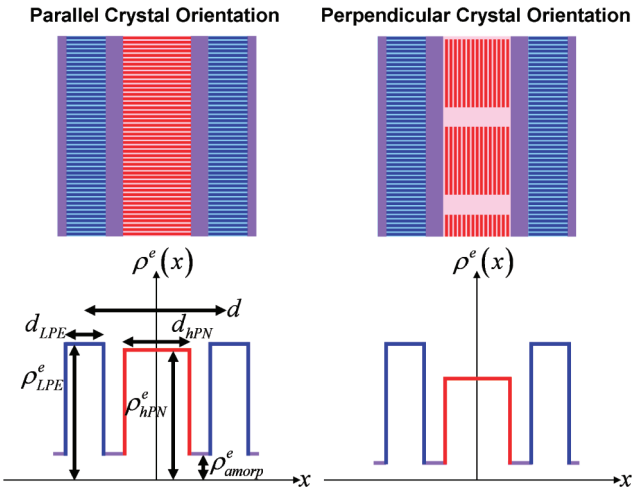

Figure 10. Schematic of three-layer square-wave model used to represent electron density profiles for parallel vs perpendicular crystal orientation in the hPN/LPE double-crystalline diblock copolymers. The electron density of the red layer is lower in the perpendicular vs parallel orientation, as it is averaged over both crystalline and amorphous hPN. Also, the electron density of the amorphous (purple) layer is lower in the perpendicular vs parallel orientation, as it is assumed to be essentially pure LPE.

diblocks, the LPE block is the first block to crystallize, and its crystallization drives the formation of a crystalline/amorphous lamellar microstructure from an initially homogeneous melt. Subsequently, either isothermally or upon further cooling, the hPN block also crystallizes between the existing LPE crystalline lamellae. This raises the question of the orientation of the hPN crystals relative to the structure-templating LPE lamellae. Unfortunately, the fiber drawing technique applied to hPN/LPE 26/26 (Figures 1 and 2) was unsuccessful for the lower molecular weight diblocks; 2D WAXS patterns obtained on fiber specimens of the three ~20 kg/mol diblocks (not shown), both as-drawn and after annealing below T_m, revealed nearly isotropic crystal orientation, indicating that the polymer chains had relaxed prior to crystallization. Consequently, we took the approach of modeling the primary SAXS peak intensity for different assumed hPN and LPE crystal orientations and then comparing the direction of the predicted intensity change (either increase or decrease) upon cooling through T_{cc} with that observed experimentally. Though the exact magnitude of the intensity change depends on structural parameters which are difficult to precisely determine in these complex polymers, the direction of the change on cooling through T_{cc} is relatively robust to modest variations (uncertainties) in these structural parameters and, as shown below, is sufficient to identify the relative crystal orientations. Two such limiting orientations were considered: as schematized in Figure 10, the second-to-crystallize hPN block (shown in red) could have its crystal stems either parallel or perpendicular to the LPE stems (shown in blue).

The SAXS intensity profiles, acquired during cooling, for hPN/LPE 9/9, 6/12, and 11/6 have been presented in Figures 5b, 6d, and 9b, respectively. Taking the symmetric diblock, hPN/LPE 9/9, as an example, we find that the crystallization of the LPE block yields a lamellar microstructure (122 and 114 °C patterns); upon cooling to 90 °C, the hPN block also crystallizes, which causes the first-order SAXS peak to both broaden and decrease in intensity. The broadening is due to additional scattering from the hPN crystallites, while the intensity reduction is the result of a decrease in electron density contrast upon hPN crystallization. As the temperature is lowered further across T_{cc} (to 50 °C), the first-order SAXS peak undergoes an additional large reduction in scattering intensity. Since the lamellar-scale morphology remains unchanged through this transition, the observed intensity reduction reflects changes in electron density contrast, principally the 1% mass density change at the hPN crystal−crystal transition. It is this observed strong intensity decrease on cooling through T_{cc} which allows us to discriminate, using the simple three-layer square-wave model, between the two limiting crystal orientations indicated in Figure 10.

For the isotropic lamellar specimens employed here, the integrated intensity of the primary SAXS peak varies as the square of the amplitude of the Fourier transform of its one-dimensional electron density profile, evaluated at q corresponding to the first-order peak.[51] In Figure 10, three distinct layers repeat along the stacking direction of the structure-templating LPE crystals: a pure LPE crystalline layer (shown in blue), an amorphous layer (shown in purple), and an hPN layer (shown in red), which may be fully crystalline, in the parallel orientation shown at left, or partially crystalline, in the perpendicular orientation shown at right. The thickness and electron density of layer i are represented by d_i and ρ^e_i, respectively. Furthermore, the boundary between the layers is assumed to be sharp. For this study, the square-wave model is used to provide only qualitative predictions of intensity changes of the first-order SAXS peak—either an increase or a decrease—as the hPN crystals pass through T_{cc}; the assumption of sharp layer interfaces does not affect this qualitative behavior. The details concerning the model and the parameter values used for the two limiting crystal orientations are described in the Supporting Information.

For two of the low molecular weight diblocks, hPN/LPE 11/6 and 9/9, a clear T_{cc} was detected upon cooling. For the hPN-rich diblock, hPN/LPE 11/6, the square-wave model indicates that only the perpendicular crystal orientation—not the parallel orientation—can yield a decrease in the first-order peak intensity across T_{cc}. For the symmetric diblock, hPN/LPE 9/9, the situation is less clear-cut, as both the perpendicular and parallel orientations are calculated to yield a reduction in SAXS primary peak intensity on cooling through T_{cc}. However, the similarity in SAXS pattern evolution for hPN/LPE 11/6 and 9/9 strongly suggests that both have a perpendicular stacking of LPE and hPN crystals. Comparing this model-deduced crystal orientation in the lower molecular weight diblocks (right schematic in Figure 10) to that observed via fiber X-ray diffraction in the higher molecular weight diblock (Figure 2c), we find that even though the identity of the templating block is switched, the overall crystalline morphology of the diblocks remains qualitatively the same: the second-to-crystallize block orients its crystals orthogonally to the first-to-crystallize block.

The qualitatively different changes predicted for the first-order SAXS peak intensity for hPN/LPE 11/6 upon cooling through T_{cc}, for the parallel vs perpendicular structures, can be understood physically as follows. The electron densities of the two crystalline phases (LPE and hPN) are closely matched, such that the electron density profile for the parallel case (at left in Figure 10) approximates a wave of period $d/2$, for which no peak at $q^* = 2\pi/d$ would be observed. The intensity calculated to remain at $q^* = 2\pi/d$ in the parallel case, when both blocks are

crystallized, reflects relatively small differences between d_{LPE} and d_{hPN}, and between ρ^e_{LPE} and ρ^e_{hPN}; thus, a further increase in ρ^e_{hPN} as the hPN crystals transition from the RD to the RO phase can produce either an increase or decrease in the intensity at $q^* = 2\pi/d$ for the parallel arrangement, depending on the precise values of d_{LPE} and d_{hPN} (and with the d_{LPE} and d_{hPN} values corresponding to hPN/LPE 11/6, a large increase is calculated). By contrast, when the hPN crystals are assumed to stack perpendicular to the LPE crystals, the electron density of the hPN layer is effectively lowered because it is averaged over both crystalline and amorphous hPN regions, as shown in the electron density profile at right in Figure 10. This then leads to a significantly reduced ρ^e_{hPN}, such that the LPE and hPN layers are no longer closely matched in electron density; when ρ^e_{hPN} increases upon cooling through T_{cc}, the scattered intensity at $q^* = 2\pi/d$ invariably decreases (for any values of d_{LPE} and d_{hPN}), as observed experimentally.

CONCLUSIONS

By exploiting the different temperature dependences of the freezing points of LPE and hPN, we have shown that the identity of the structure-templating (first-to-crystallize) block in double-crystalline hPN/LPE diblocks can be switched simply by changing the total molecular weight. Specifically, in symmetric hPN/LPE, while hPN is the structure-templating block at 50 kg/mol diblock molecular weight, LPE is the structure-templating block in 20 kg/mol diblocks. Additionally, the relative orientation of the hPN and LPE crystals in both high- and low-molecular-weight hPN/LPE diblocks was investigated. In all cases, the crystals stack orthogonally: the second-to-crystallize block, which crystallizes in confinement, orients its crystal stems perpendicular to those in the first-to-crystallize block. This crystal orientation is analogous to that most frequently observed when crystallization is confined between glassy lamellae. However, unlike the case for crystalline/glassy diblocks, the ability to tune the crystallization sequence of the two blocks in hPN/LPE (and thus which block crystallizes in confinement, with the perpendicular orientation) through molecular weight allows a range of structures to be produced with a single diblock chemistry.

ASSOCIATED CONTENT

Supporting Information. Fiber X-ray diffraction pattern for hPN/LPE 26/26 at T = 138 °C; selected WAXS patterns matched to the simultaneous heating thermogram for hPN/LPE 9/9 and 6/12; detailed description of the three-layer square-wave model; electron density values for amorphous and crystalline LPE and hPN; structural parameter values used in square-wave model calculations for the parallel and perpendicular crystal orientations. This material is available free of charge via the Internet at http://pubs.acs.org.

AUTHOR INFORMATION

Corresponding Author

*E-mail: register@princeton.edu.

Present Addresses

[†]3M Corporate Research Process Laboratory, St. Paul, MN 55144.

ACKNOWLEDGMENT

This work was generously supported by the National Science Foundation, Polymers Program (DMR-1003942). The synchrotron X-ray experiments were performed at the DuPont–Northwestern–Dow Collaborative Access Team (DND-CAT) beamline, located at Sector 5 of the Advanced Photon Source (APS). DND-CAT is supported by E. I. Dupont de Nemours & Co., the Dow Chemical Company, and the State of Illinois. Use of the APS was supported by the U.S. Department of Energy, Office of Science, Office of Basic Energy Sciences, under Contract DE-AC02-06CH11357. The authors gratefully acknowledge Brian Landes (Dow Chemical) and Steven Weigand (DND-CAT) for assistance with X-ray scattering experiments.

REFERENCES

(1) Bates, F. S.; Fredrickson, G. H. *Phys. Today* **1999**, *52*, 32–38.
(2) Hamley, I. W. *Adv. Polym. Sci.* **1999**, *148*, 113–137.
(3) Loo, Y. L.; Register, R. A. Crystallization Within Block Copolymer Mesophases. In *Development in Block Copolymer Science and Technology*; Hamley, I. W., Ed.; John Wiley & Sons, Ltd.: Chichester, 2004; pp 213–243.
(4) Muller, A. J.; Balsamo, V.; Arnal, M. L. *Adv. Polym. Sci.* **2005**, *190*, 1–63.
(5) Rangarajan, P.; Register, R. A.; Fetters, L. J. *Macromolecules* **1993**, *26*, 4640–4645.
(6) Lee, L.-B. W.; Register, R. A. *Macromolecules* **2004**, *37*, 7278–7284.
(7) Nojima, S.; Kato, K.; Yamamoto, S.; Ashida, T. *Macromolecules* **1992**, *25*, 2237–2242.
(8) Rangarajan, P.; Register, R. A.; Fetters, L. J.; Bras, W.; Naylor, S.; Ryan, A. J. *Macromolecules* **1995**, *28*, 4932–4938.
(9) DiMarzio, E. A.; Guttman, C. M.; Hoffman, J. D. *Macromolecules* **1980**, *13*, 1194–1198.
(10) Whitmore, M. D.; Noolandi, J. *Macromolecules* **1988**, *21*, 1482–1496.
(11) Quiram, D. J.; Register, R. A.; Marchand, G. R. *Macromolecules* **1997**, *30*, 4551–4558.
(12) Loo, Y. L.; Register, R. A.; Ryan, A. J. *Phys. Rev. Lett.* **2000**, *84*, 4120–4123.
(13) Zhu, L.; Chen, Y.; Zhang, A. Q.; Calhoun, B. H.; Chun, M. S.; Quirk, R. P.; Cheng, S. Z. D.; Hsiao, B. S.; Yeh, F. J.; Hashimoto, T. *Phys. Rev. B* **1999**, *60*, 10022–10031.
(14) Loo, Y. L.; Register, R. A.; Adamson, D. H. *J. Polym. Sci., Part B: Polym. Phys.* **2000**, *38*, 2564–2570.
(15) Douzinas, K. C.; Cohen, R. E. *Macromolecules* **1992**, *25*, 5030–5035.
(16) Cohen, R. E.; Bellare, A.; Drzewinski, M. A. *Macromolecules* **1994**, *27*, 2321–2323.
(17) Hamley, I. W.; Fairclough, J. P. A.; Terrill, N. J.; Ryan, A. J.; Lipic, P. M.; Bates, F. S.; Towns-Andrews, E. *Macromolecules* **1996**, *29*, 8835–8843.
(18) Zhu, L.; Cheng, S. Z. D.; Calhoun, B. H.; Ge, Q.; Quirk, R. P.; Thomas, E. L.; Hsiao, B. S.; Yeh, F. J.; Lotz, B. *J. Am. Chem. Soc.* **2000**, *122*, 5957–5967.
(19) Zhu, L.; Calhoun, B. H.; Ge, Q.; Quirk, R. P.; Cheng, S. Z. D.; Thomas, E. L.; Hsiao, B. S.; Yeh, F.; Liu, L. Z.; Lotz, B. *Macromolecules* **2001**, *34*, 1244–1251.
(20) Zhu, L.; Cheng, S. Z. D.; Calhoun, B. H.; Ge, Q.; Quirk, R. P.; Thomas, E. L.; Hsiao, B. S.; Yeh, F.; Lotz, B. *Polymer* **2001**, *42*, 5829–5839.
(21) Muller, A. J.; Arnal, M. L.; Balsamo, V. *Lect. Notes Phys.* **2007**, *714*, 229–259.
(22) Hamley, I. W.; Castelletto, V.; Castillo, R. V.; Muller, A. J.; Martin, C. M.; Pollet, E.; Dubois, P. *Macromolecules* **2005**, *38*, 463–472.
(23) Hamley, I. W.; Parras, P.; Castelletto, V.; Castillo, R. V.; Muller, A. J.; Pollet, E.; Dubois, P.; Martin, C. M. *Macromol. Chem. Phys.* **2006**, *207*, 941–953.

(24) Nojima, S.; Akutsu, Y.; Washino, A.; Tanimoto, S. *Polymer* **2004**, *45*, 7317–7324.
(25) Nojima, S.; Akutsu, Y.; Akaba, M.; Tanimoto, S. *Polymer* **2005**, *46*, 4060–4067.
(26) Higa, T.; Nagakura, H.; Sakurai, T.; Nojima, S. *Polymer* **2010**, *51*, 5576–5584.
(27) Perret, R.; Skoulios, A. *Makromol. Chem.* **1972**, *162*, 147–162.
(28) Perret, R.; Skoulios, A. *Makromol. Chem.* **1972**, *162*, 163–177.
(29) Takeshita, H.; Fukumoto, K.; Ohnishi, T.; Ohkubo, T.; Miya, M.; Takenaka, K.; Shiomi, T. *Polymer* **2006**, *47*, 8210–8218.
(30) Jiang, S.; He, C.; Men, Y.; Chen, X.; An, L.; Funari, S. S.; Chan, C. *Eur. Phys. J. E* **2008**, *27*, 357–364.
(31) He, C. L.; Sun, J.; Deng, C.; Zhao, T.; Deng, M. X.; Chen, X. S.; Jing, X. B. *Biomacromolecules* **2004**, *5*, 2042–2047.
(32) He, C.; Sun, J.; Ma, J.; Chen, X.; Jing, X. *Biomacromolecules* **2006**, *7*, 3482–3489.
(33) Myers, S. B.; Register, R. A. *Macromolecules* **2008**, *41*, 6773–6779.
(34) Cho, T. Y.; Heck, B.; Strobl, G. *Colloid Polym. Sci.* **2004**, *282*, 825–832.
(35) Myers, S. B.; Register, R. A. *Macromolecules* **2010**, *43*, 393–401.
(36) Trzaska, S. T.; Lee, L. B. W.; Register, R. A. *Macromolecules* **2000**, *33*, 9215–9221.
(37) Lee, L.-B. W.; Register, R. A. *Macromolecules* **2005**, *38*, 1216–1222.
(38) Bishop, J. P.; Register, R. A. *J. Polym. Sci., Part B: Polym. Phys.* **2011**, *49*, 68–79.
(39) Lee, L.-B. W. Ph.D. Thesis, Princeton University, 2004.
(40) Quirk, R. P.; Alsamarraie, M. A. A. In *Polymer Handbook*, 3rd ed.; Brandrup, J., Immergut, E. H., Eds.; Wiley: New York, 1989; p V/15.
(41) Dean, D. M.; Rebenfeld, L.; Register, R. A.; Hsiao, B. S. *J. Mater. Sci.* **1998**, *33*, 4797–4812.
(42) Loo, Y. L.; Register, R. A.; Ryan, A. J.; Dee, G. T. *Macromolecules* **2001**, *34*, 8968–8977.
(43) Ueda, M.; Register, R. A. *J. Macromol. Sci., Phys.* **1996**, *B35*, 23–36.
(44) Shibayama, M.; Hashimoto, T. *Macromolecules* **1986**, *19*, 740–749.
(45) Porod, G. In *Small-Angle X-ray Scattering*; Glatter, O., Kratky, O., Eds.; Academic Press: London, 1982.
(46) Albuerne, J.; Marquez, L.; Muller, A. J.; Raquez, J. M.; Degee, P.; Dubois, P.; Castelletto, V.; Hamley, I. W. *Macromolecules* **2003**, *36*, 1633–1644.
(47) Muller, A. J.; Albuerne, J.; Esteves, L. M.; Marquez, L.; Raquez, J. M.; Degee, P.; Dubois, P.; Collins, S.; Hamley, I. W. *Macromol. Symp.* **2004**, *215*, 369–382.
(48) Muller, A. J.; Albuerne, J.; Marquez, L.; Raquez, J. M.; Degee, P.; Dubois, P.; Hobbs, J.; Hamley, I. W. *Faraday Discuss.* **2005**, *128*, 231–252.
(49) Bair, H. E.; Huseby, T. W.; Salovey, R. *Polym. Prepr. (Am. Chem. Soc., Div. Polym. Chem.)* **1968**, *9*, 795–805.
(50) Stribeck, N. *Colloid Polym. Sci.* **1993**, *271*, 1007–1023.
(51) Roe, R. J. *Methods of X-Ray and Neutron Scattering in Polymer Science*; Oxford University Press: New York, 2000.